THE UNIVERSITY *of* EDINBURGH

Edinburgh Research Explorer

On the use of CFD for the design of yacht hulls

Link:
Link to publication record in Edinburgh Research Explorer

Document Version:
Publisher's PDF, also known as Version of record

Published In:
Transactions of the Royal Institution of Naval Architects Part B: International Journal of Small Craft Technology

OPEN ACCESS

ON THE USE OF CFD FOR THE DESIGN OF YACHT HULLS

I M Viola, Institute for Energy Systems, School of Engineering, The University of Edinburgh, UK, **S Bartesaghi**, Former PhD student at the Mechanical Engineering Department, Politecnico di Milano, Italy, **S Della Rosa,** Silverio Della Rosa Naval Architect, Italy, and **S Cutolo,** Hydro Tec, Italy

SUMMARY

There are three main methods to assess the hydrodynamic characteristics of yachts, namely, viscous and inviscid numerical analysis, and experimental tests. Computational tools are now widely used in yacht design because of the rapid growth of high-powered computers during the last ten years. Viscous computational fluid dynamic codes are now one of the most important tools in design offices, in marine and other fields, and in some fields they have completely replaced inviscid codes and experimental tests. A deeper awareness of the uncertainty of RANS code results is necessary, achievable with a rigorous application of a verification and validation process. The effectiveness of numerical methods is discussed with regards to their application to yacht design. Potentialities and limitations of numerical methods are discussed showing that these must be used with caution, so as to provide a reliable suite of design tools.

1. INTRODUCTION

Two hundred years ago the design of vessels was mainly based on the experience of the designer and rarely on experimental measurements. In 1874, William Froude [1] recognised that the limitation of towing tank tests is the impossibility of modelling at the same time the full-scale ratio between inertial and viscous forces, namely the Reynolds number (Re), and the ratio between inertial and gravitational forces, namely the Froude number (Fr). It is common practice to scale the model in order to perform the test at the same Fr than in full scale. The measured total resistance is considered to be made of a component due to the wave generation, namely *wave resistance*, and a component due to the viscous effects, namely *viscous resistance*. It is also assumed that the wave resistance is mainly affected by Fr, while the viscous resistance is mainly affected by Re. Therefore the measured resistance is corrected a posteriori to take into account that the viscous resistance in full scale must be different from model scale being tested at a different Re. The studies by Prandtl [2] and by his students Von Karman [3] and Blasius [4], led to great insight about the boundary layer on flat plates. These studies allowed estimating the viscous resistance with several empirical formulations derived from measurements on flat plates. The curvature of the hull was then taken into account by further formulations developed in the 1950s [5, 6, 7]. It is interesting to note that these formulations are still in use today to correlate the model-scale resistance measured in the towing tank with the full-scale resistance.

In the 1970s, greatly improved computers allowed potential flow theory to be successfully applied in marine applications. This theory assumes the flow to be inviscid and irrotational, and allows modelling of non-dissipative flows. For instance, the lift generated by airfoils at angle of attack below the stall angle and the wave pattern generated by a vessel can be modelled with potential flow. Therefore, the wave resistance can be computed but the viscous resistance must be estimated with other methods.

The fluid dynamic equations, which take into account viscous effects, were developed in 1822 by Claude-Louis Navier [8] and then completed by Sir George Gabriel Stokes [9]. These equations, known as Navier-Stokes equations, are very difficult do solve and only few analytical solutions are possible. For complex geometries, such as a hulls, a propellers, etc., the equations must be solved numerically (i.e. iterating through approximate solutions). The computational effort to solve them numerically depends on Re. At high Re the flow is turbulent and the turbulent fluctuations have a significant effect on the mean flow field. Therefore, the turbulent fluctuations must be taken into account in order to compute the mean flow field and, for instance, the resulting mean hull resistance. The largest turbulent structures are of the order of magnitude of the hull length L, and these break into smaller structures until dissipated by viscous effect. The higher the Re, the greater the difference between the smallest and the largest turbulent scales, and thus the higher the needed spatial resolution and the more computationally demanding to solve the Navier-Stokes equations. Moreover, the smaller the turbulent structure then the shorter the oscillation of the velocity and pressure. Therefore, both the spatial and the time discretization should allow all the turbulent scales to be modelled. Such a simulation is very computationally demanding and it is called Direct Numerical Simulation (DNS). For instance, in 1988, Spalart [10] performed a milestone DNS of a turbulent flat-plate boundary layer up to Re=1400. Today, higher Re can be modeled but it is still impossible to perform DNS at the high Re values of interest to naval architects.

If the spatial and time resolutions do not allow all the turbulent scales to be modelled, then the filtered scales must be taken into account by semi-empirical models. It is possible to perform a low-resolution Navier-Stokes simulation, but significant empiricism must be introduced. For instance, if a Reynolds Averaged Navier Stokes (RANS) simulation is performed, the filtered scales are taken into account by the so called *turbulence model*, which is a non-universal formulation and its

coefficients are achieved with experiments on simplified test cases.

For the high *Re* values of interest to naval architects, RANS is the most common solution. However, also RANS needs a significant computational effort compared to potential flow. During most of the 20th century the Navier-Stokes equations could be solved only for simple geometries and low *Re*, such as for blood flowing through arteries. At the end of the 20th century, the growth of computational resources allowed higher spatial and time resolutions to be achieved and higher *Re* to be modelled.

The correlation between the spatial resolution increase and the growth of the computational resources is well illustrated by the following example on sail aerodynamics. In fact, while sail aerodynamics presents different challenges from hull hydrodynamics, the correlation between spatial resolution and the growth of the computational resources is similar in these two fields. Figures 1,2 show the velocity of the fastest computers in the world in gigaflops and the number of cells used in downwind sail aerodynamics from 1995 to 2008, respectively. Note that the same scales are used for the axes of the two figures. The grow rate of both the computational resources and of the spatial resolution is about one order of magnitude every three years. After the first application by Hedges in 1993 [11], Miyata performed a milestone simulation in 1999 [12]. Then, during the 31st and the 32nd America's Cup, the top challengers used grids with a number of cells of the order of 10^5 and 10^7 respectively. In 2008, Viola [13] performed a milestone simulation of 37 millions elements and, in the same year, Viola & Ponzini [14] performed the largest grid ever done reaching a billion cells.

This example clearly shows that the spatial resolution used in RANS applications will certainly increase in the future together with the grown of the computational capability. The higher the number of cells of the grid, the higher is the spatial resolution and thus the less the simulation relies on the turbulence model, which is a non-universal semi-empirical formulation. The increase in the spatial and time resolutions will also allow different techniques for solving the Navier-Stokes equations to be efficiently used in the design process, such as Detached Eddy Simulation (DES) and Large Eddy Simulations (LES), which are too time consuming at the current state of the art.

RANS codes were used since the 1980s for stern/wake flows but only in 1994 a significant number of codes modelling the free surface were presented in a conference: the Computational Fluid Dynamics (CFD) Workshop in Tokyo [15]. Most of these codes used the *interface tracking* techniques, which require the grid to follow the free surface and cannot model breaking waves. Later in the 1990s, more flexible *interface capturing* techniques with a *volume of fluid* approach

[16] were widely implemented opening to a wider range of applications. In 1997 Orihara and Miyata [17] performed a free to sink and trim simulation of a semi-planning boat, while Miyata *et al.* [18] performed a free to sink, trim and heel sailing yacht. In 2001 Azcueta [19] performed 6 degree of freedom (DOF) simulations.
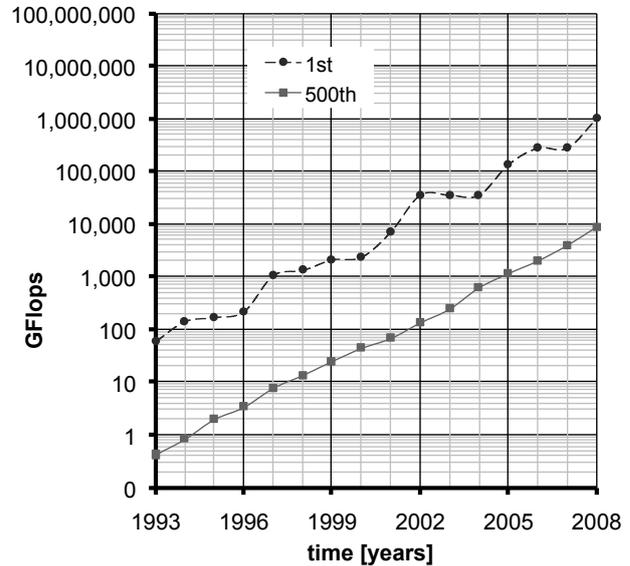

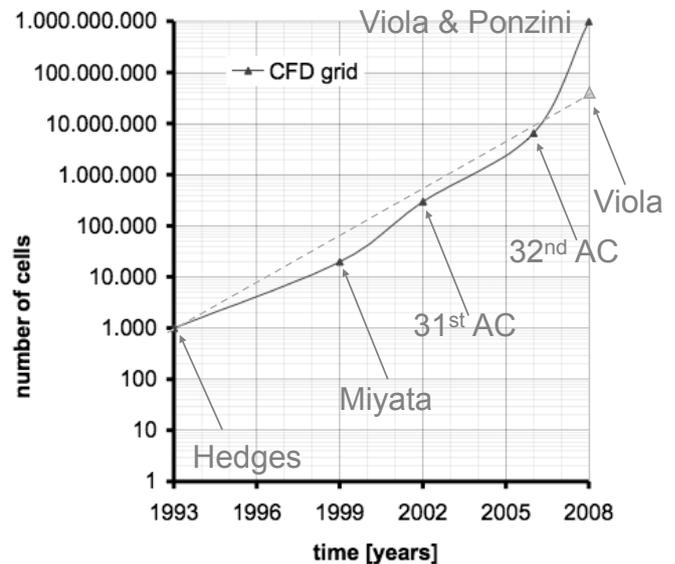Figure 1: Speed of the 1st and 500th fastest computer in the world (data from top500.org).

Figure 2: Maximum number of cells used in RANS simulations for sail aerodynamics.

RANS simulations in the marine fields have become much more widely used during the last decade. The state of the art is well presented by the *CFD Workshop Tokyo 2005* [20] and the *Gothenburg 2010: A Workshop on CFD in Ship Hydrodynamics* [21], where the impact of RANS in ship hydrodynamics was discussed. It was noted that it is successfully extending to the prediction of

6 DOF ship motions for seakeeping and manoeuvrability. However, the RANS capability of accurately modelling large amplitude ship motions like stall and the interactions between hull and appendages was discussed.

CFD users are increasingly aware of the need of verification and validation (V&V) procedures, in particular for unsteady forces in time domain. Conversely, V&V has been often ignored in the yacht and superyacht field. While a significant effort has been spent on exploring the modelling capabilities of RANS, not enough effort has been spent on verifying and validating the results. Moreover, validation has been often misleading by the lack of verification. Incorrect results have led to scepticism about RANS capabilities. Conversely, the authors are enthusiastic about it, as long as the uncertainty of the solution is always carefully explored and taken into account by the designer.

The different methods to assess the hydrodynamic characteristics of yachts, namely, viscous and inviscid numerical analysis, and experimental tests, are discussed hereafter. The aim of this paper is to highlight how the results can be interpreted correctly only if paired with their correlated uncertainties. In particular, due to the increasing use of RANS, the paper focuses on the verification and validation of the results achieved with RANS, showing how the results of this process should be interpreted.

2. EXAMPLE OF RANS APPLICATION

The bare hull of a 105-foot motor yacht (Figure. 3) was modelled with the finite-volume code STAR-CCM+ (CD-adapco). The hull was designed by Hydro Tec and launched in July 2012. The simulations were performed both in model scale and in full scale, and the results were compared with towing tank tests.

Zero yaw and heel was considered and thus only half of the yacht was modelled taking advantage of the yacht symmetry, allowing using a domain 4L long, 1.8L high and 1.5L deep. Two different grids of hexahedral cells were performed for model-scale and full-scale simulations in order to achieve an averaged y+ along the hull of 80 in both conditions. Both grids were made of less than one million cells oriented with the boat axis and trimmed by the boat surface. The simulations run in few hours on a standard multi-core processor.

A RANS simulation was performed using the $k - \epsilon$ *realizable* model and *two-layer all-y+* [22] wall function. The Volume Of Fluid (VOF) approach was used to model the two phases and a High Resolution Interface Capturing (HRIC) interpolation scheme was used to model the free surface. A constant velocity V was used at the inlet with 1% turbulence intensity and turbulent/physical viscosity ratio of 10. The model was both physically tested and numerically modelled in free to sink and trim condition. The grid was rigidly moved

with respect to the boundary conditions in order to take into account the sink and trim movements. For more details about the numerics see the 6DOF model implemented in STAR-CCM+ (CD-adapco). Time steps of 0.02s were used and 200s were modelled.

Figure 3: Photograph of the 105-foot motor-yacht tested.

Figure 4 shows the numerical ('*NUM*') and the experimental ('*EXP*') resistance coefficient C_T at model scale versus *Fr*, where:

$$C_T = \frac{R}{\frac{1}{2}\rho V^2 A_W} \tag{1}$$

R is the resistance, ρ is the density of the water, A_W is the wetted surface.
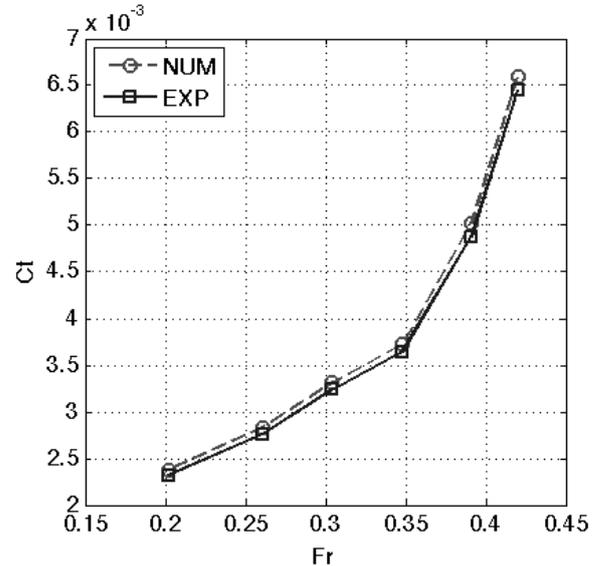

Figure 4: Numerical and experimental C_T at model scale.

Figures 5 shows the numerical and the experimental trim at model scale.

The model-scale experimental results were corrected with the ITTC'57 model-ship correlation line [7] in order to achieve the full-scale resistance. Table 1 shows the corrected experimental resistance coefficient and the numerical resistance computed at

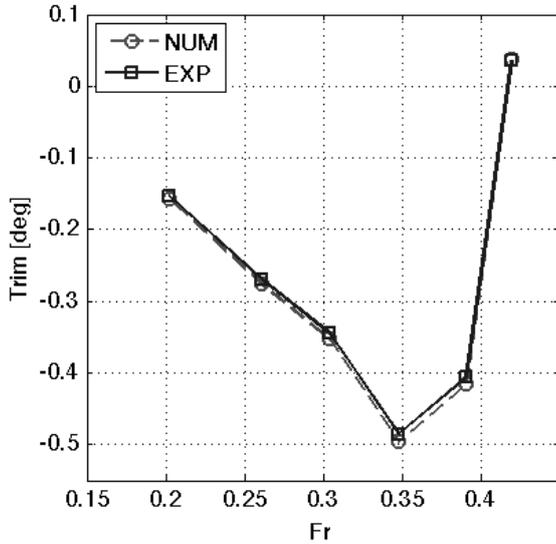full-scale. The comparison is performed at the design speed ($Fr = 0.395$).

Figure 5: Num. and exp. trim at model scale.

Table 1: Full-scale C_T at $Fr = 0.395$.

$C_{T\,EXP}$	$9.684 \cdot 10^{-3}$
$C_{T\,num}$	$9.815 \cdot 10^{-3}$
$(C_{T\,num} - C_{T\,EXP})/C_{T\,EXP}$	$+ 1.33\%$

The numerical and experimental results are in very good agreement both in model scale and in full scale. The maximum numerical-experimental difference is about 3.1% and 1.3% in model scale and full scale respectively for the resistance, while the maximum differences in the trim is 0.01 degrees in model scale.

It is interesting to note that the trim increases of about 0.1 degree at $Fr = 0.395$ when the simulation is performed in full scale instead of model scale.

3   VERIFICATION AND VALIDATION

As explained above, RANS requires the turbulence model to estimate the effect of the spatial and temporal filtered fluctuations on the averaged velocity and pressure fields. Therefore, the solution does necessarily depend upon both the spatial and time discretization, and on the turbulence model. A numerical solution also depends on the algorithms used to estimate the solution at the successive iteration. Moreover a converging iteration process tends towards a solution, but a finite number of iterations led necessary to a difference between it and the actual solution. Finally, the geometry and the conditions modelled numerically are inevitably slightly different from the real geometry, which is usually more detailed, and also the real conditions, which usually have more dynamics than which is modelled. Therefore there are many sources of errors and the uncertainty of the solution must be evaluated. It should

be noted that also potential flow codes and experimental techniques have various sources of errors and the uncertainty must be equally considered.

The validation and verification (V&V) process was initiated by Roache in 1994 [23] with the grid converge index to estimate the uncertainty due to the spatial and temporal discretization. Guidelines for V&V were developed by the American Institute of Aeronautics and Astronautics (AIAA) Committee on Standards for CFD [24, 25], by the American Society of Mechanical Engineers (ASME) in 2009 [26, 27], and by the International Towing Tank Conference (ITTC) Specialist Committee on CFD [28]. Also, Viola *et al.* recently published guidelines with an example test case on yacht sail aerodynamics [29]. These guidelines are used as reference in the present paper.

3.1   NUMERICAL AND MODELLING UNCERTAINTIES

The difference between the computed value ϕ_{CFD} and the true value ϕ_{TRUE} is the simulation error δ_ϕ. This is due to the numerical error $\delta_{\phi_{num}}$ and to the modelling error $\delta_{\phi_{mod}}$. The numerical error includes errors due to the spatial resolution (grid), the temporal resolution (time step), the round-off due to the precision of the machine, various other input parameters and the convergence of the iterative process. The modelling error includes errors due to the choice of the equations, boundary and initial conditions, such as, for instance, the turbulence model and the dimension of the domain.

$$\delta_\phi = \phi_{CFD} - \phi_{TRUE} = \delta_{\phi_{num}} + \delta_{\phi_{mod}} \qquad (2)$$

The verification process assesses the numerical uncertainty $U_{\phi_{num}}$ at 95% confidence level due to the numerical error $\delta_{\phi_{num}}$, while the validation process assesses the modelling uncertainty $U_{\phi_{mod}}$ due to the modelling error $\delta_{\phi_{mod}}$.

In particular, the verification process assesses the uncertainty components due to the grid size U_{ϕ_g}, time step U_{ϕ_t}, round-off U_{ϕ_r}, other input parameters U_{ϕ_p}, and convergence U_{ϕ_c}. The numerical uncertainty $U_{\phi_{num}}$ is estimated as per experimental fluid dynamics uncertainty analysis:

$$U_{\phi_{num}} = \sqrt{U_{\phi_g}^2 + U_{\phi_t}^2 + U_{\phi_r}^2 + U_{\phi_p}^2} + U_{\phi_c} \qquad (3)$$

Often the largest uncertainties are due to the grid size U_{ϕ_g}, time step U_{ϕ_t} and convergence U_{ϕ_c}. These uncertainties are evaluated performing several simulations with different grid sizes and time steps. Increasing the spatial and temporal resolutions, the solution should converge (monotonically or oscillating)

to a grid- and time-independent solution. Too coarse grids and too large time steps lead to non-converging trends and larger uncertainties.

The validation is performed comparing the numerical solution ϕ_{CFD} with the experimental results ϕ_{EXP}. The uncertainty of the validation $U_{\phi_{val}}$ is due to the numerical uncertainty $U_{\phi_{EXP}}$ and to the experimental uncertainty $U_{\phi_{EXP}}$:

$$U_{\phi_{val}} = \sqrt{U_{\phi_{num}}^2 + U_{\phi_{EXP}}^2} \tag{4}$$

The estimate of ϕ *is validated at the level of* $U_{\phi_{val}}$ if the absolute value of the error $|\delta_\phi| = |\phi_{CFD} - \phi_{TRUE}|$ is smaller than the validation uncertainty $U_{\phi_{val}}$. In fact, the validation uncertainty is a measure of the 'noise' in the comparison between the numerical and experimental data. If the error is lower than the noise - and ϕ is validated - than no conclusions can be drawn about the modelling error. Conversely, if the error is larger than the noise - and the ϕ is not validated – than the error is (partially) due to modelling error.

For a design prospective, both validated and non-validated solutions can be used. In fact, if the modelling error is estimated, it could be sufficiently small to be neglected for design purpose. Conversely, the solution could be validated thanks to a very large numerical uncertainty. While the designer is often interested in the amplitude of the numerical error, they often underestimate the importance of the verification process, i.e. of the numerical uncertainty. A numerical simulation should always be presented with the results of the verification process, and that the numerical and modelling uncertainties should always be taken into account together with the simulation results in the design process.

3.2 GRID AND TIME-STEP UNCERTAINTIES

A verification analysis of the full-scale simulation presented in Section 2 was performed. The grid size and the time step used in these simulations were used as base values, while different grid sizes and time steps were tested only at $Fr = 0.395$, where uncertainties were computed for C_t, sink and trim. In particular, the values achieved with every grid size and time step were divided by the base value achieved with the base grid size and base time step. Therefore, the following three ratios were considered:

$$\phi_1 = \frac{C_t}{C_{t_{base}}}, \qquad \phi_2 = \frac{\text{Sink}}{\text{Sink}_{base}}, \qquad \phi_3 = \frac{\text{Trim}}{\text{Trim}_{base}}$$

The *grid relative step ratio, h_g*, is defined as the ratio between the representative node distance of the current grid and of the base grid. One finer grid and one coarser grid were tested. Therefore, for the three grids, $h_g = 0.65, 1, 1.60$ respectively.

Three time steps were also investigated. In particular, the time step was halved and doubled. Therefore, the *time relative step ratio, h_t*, which is defined as the ratio between the current time step and the base time step, is $h_t = 0.5, 1, 2$ for the three simulations, respectively.

For each $\phi = \phi_1, \phi_2, \phi_3$, the trends with the relative step size $h = h_g, h_t$, are considered. The trends are fitted with Eq. (5), where the parameters c, p and ϕ_0 are computed by means of least squared method.

$$\phi(h) = c\, h^p + \phi_0 \tag{5}$$

If $p \geq 0.95$, then the uncertainty U_{ϕ_h} in the computation of ϕ due to the relative step size h is computed with Eq. (6) at 95% confidence level.

$$U_{\phi_h} = 1.25\, |\phi_h - \phi_0| + \sigma \tag{6}$$

where σ is the standard deviation of the fit error. In the present example $\sigma = 0$ because only three relative step sizes are used to compute the parameters c, p and ϕ_0.

If $p < 0.95$, then the uncertainty U_{ϕ_h} is computed with Eq. (7).

$$U_{\phi_h} = 1.5\, \frac{\phi_{max} - \phi_{min}}{1 - \frac{h_{min}}{h_{max}}} + \sigma \tag{7}$$

The grid refinement (Figure. 6) shows that the resistance coefficient ratio ϕ_1 does not show a convergent trend increasing the grid resolution (decreasing h) and therefore the uncertainty U_{ϕ_1} is computed with Eq. (7). The uncertainty, which is showed by the error bar, is larger than 12%. As a reference, dotted lines show the band within two standard deviations of the ϕ_1 distribution.

Interestingly, while a first incorrect interpretation of the results presented in Section 2 suggested that the resistance was computed within an "accuracy" of $\pm 1.33\%$ (Table 1), Figure. 6 shows that the "accuracy" is lower than $\pm 12\%$, and the contribution of the following time and convergence analysis will lead to an even larger uncertainty.

Figure 7 shows that the sink ratio ϕ_2 converges with refined grids with $p = 4.8$ and therefore the uncertainty can be computed with Eq. (6). However, the current

simulations were performed with discretisation schemes as accurate as the second orders, therefore an order of convergence higher than two is suspicious and more simulations with different grid resolutions should be performed to verify the estimate. On the other hand, the maximum difference between the trims is of the order of 0.1%, while the convergence uncertainty, which is presented in Section 3.3, is higher than 2.5%. Therefore, for the sink, it is foreseeable that the contribution of the grid uncertainty is negligible compared to the contribution of the convergence uncertainty.

As for the resistance, the trim does not present a convergent trend with the grid resolution (Figure. 8) and the uncertainty is computed with Eq. (7). Similarly, the resistance, the trim and the sink do not present convergent trims with the time resolution (Figures 9-11) and the uncertainties are computed with Eq. (7).

Table 2 summarises the orders of convergence for the resistance, trim and sink, due to the grid and time resolutions, while the uncertainties are summarised in Section 3.4 (Table 3) together with the convergence uncertainties.

Figure 7: Sink vs spatial resolution

Table 2: Uncertainties and orders of convergence

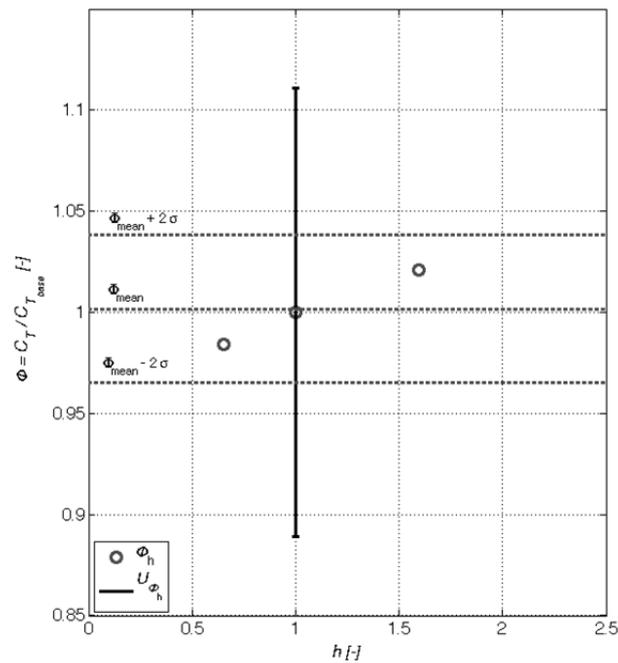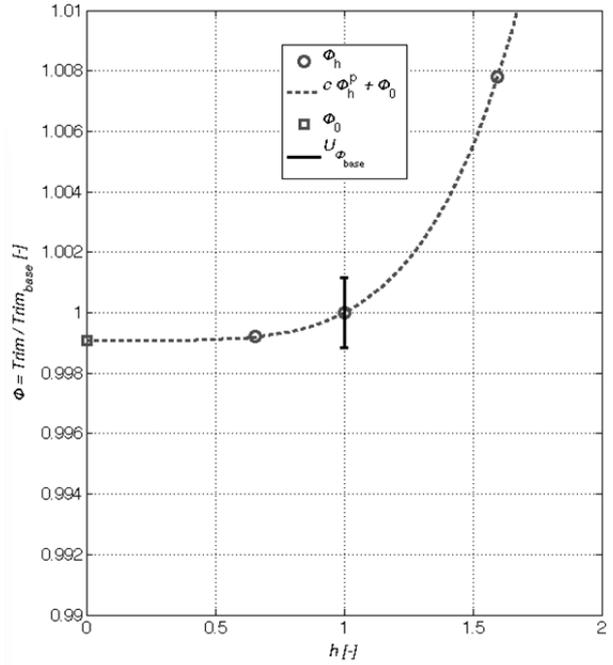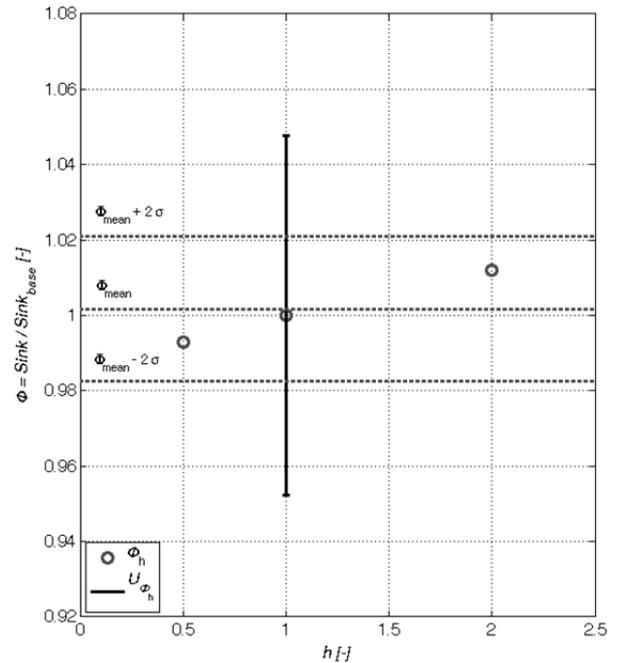|	$\phi_1 = \dfrac{C_t}{C_{t\,base}}$	$\phi_2 = \dfrac{Sink}{Sink_{base}}$	$\phi_3 = \dfrac{Trim}{Trim_{base}}$
p_g	-0.088	-0.001	4.809
p_t	-0.183	-0.082	0.185

Figure 8: Trim vs spatial resolution

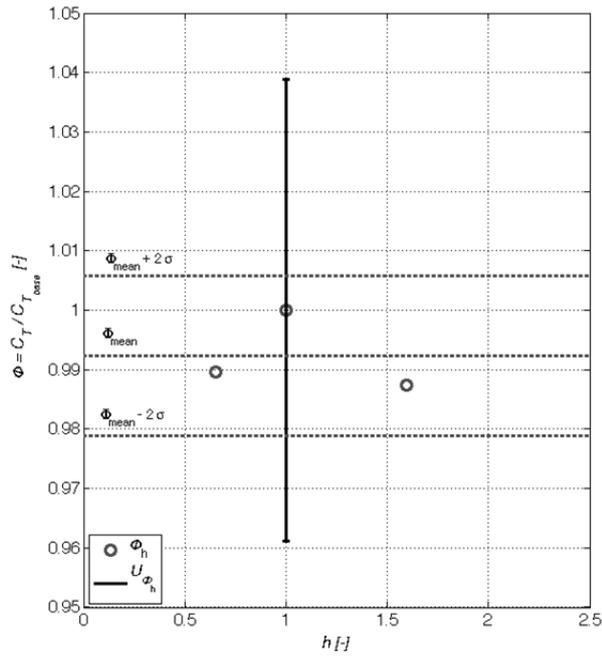Figure 6: Resistance vs spatial resolution

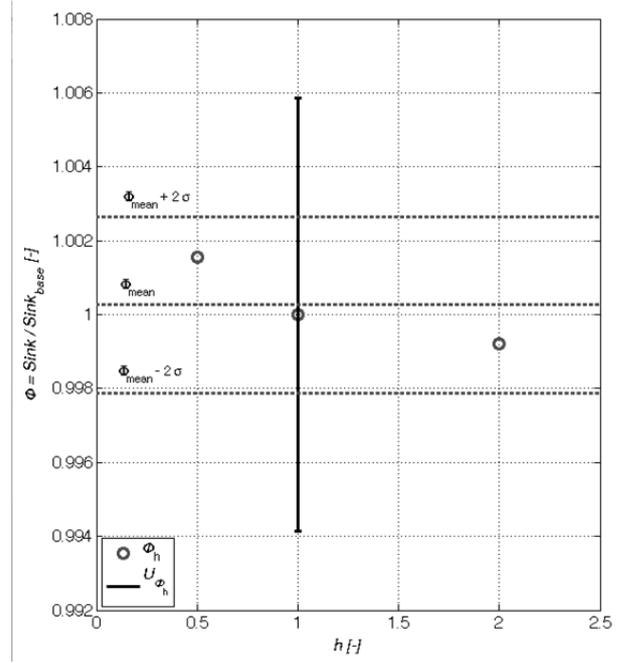Figure 9: Resistance vs time resolution
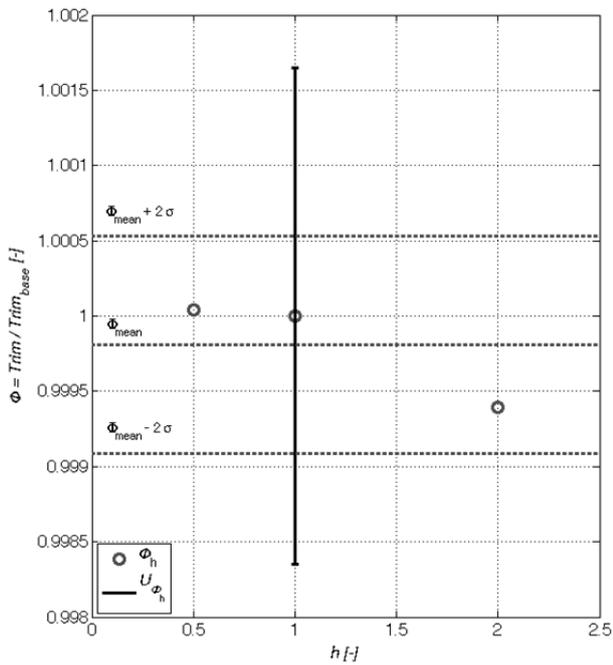

Figure 11: Trim vs time resolution
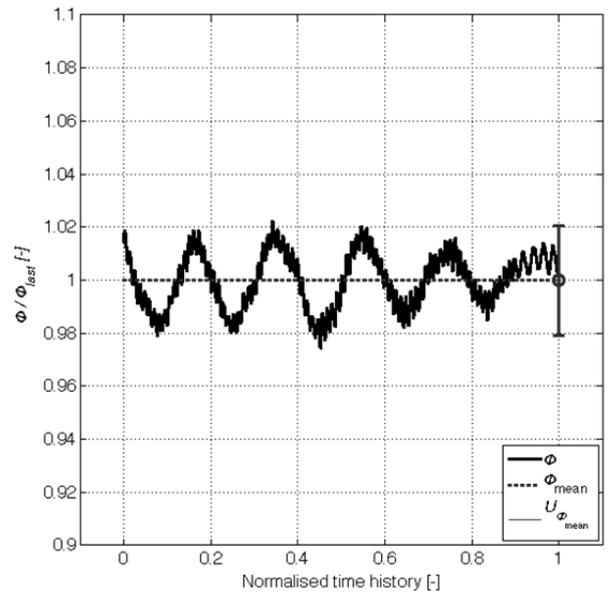

Figure 10: Sink vs time resolution

Figure 12: Convergence of the resistance

3.3 CONVERGENCE UNCERTAINTIES

The convergence in ship resistance simulations is usually more rapid than in sailing yacht aerodynamics [29]. Also, when free to sink and trim condition is modelled, wave reflection on the boundaries leads to oscillatory convergence [30]. Therefore using a least square fit, as suggested by the V&V guidelines for sail aerodynamics [29], are not practical for this type of simulations.

In the present example, 200s were computed for all simulations. After 100s, the time histories of the resistance, the sink and the trim showed oscillating trends. The convergence uncertainty at 95% confidence level was computed as twice the standard deviation of these trends over the range between 100s and 200s.
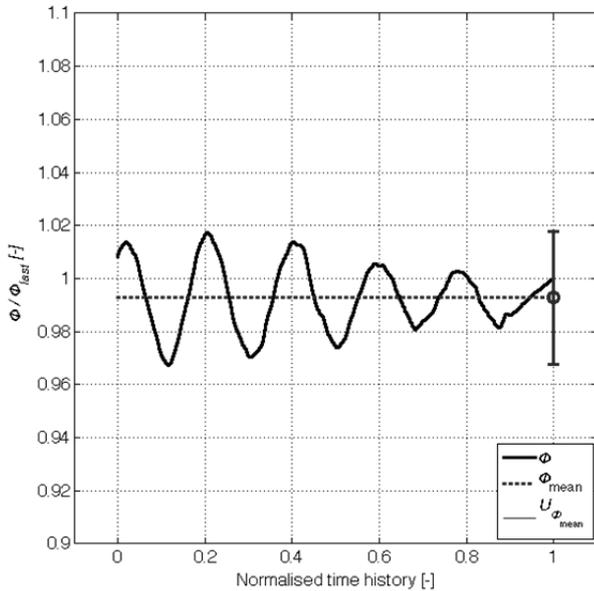

Figure 13: Convergence of the sink

Figure 12 shows the time history from 100s to 200s, normalised from zero to one, of the resistance. In particular, the resistance is divided by the last computed value in order to present a non-dimensional convergence uncertainty (error bar). It is important to note that the mean values are used as CFD results ϕ_{CFD}, and not the last computed values. The uncertainty is thus associated to the mean value (dotted line).

Similarly, Figures 13,14 show the convergence of the sink and trim ratios versus the normalised time history from 100s to 200s.

This approach suggests that the simulation can be interrupted at any stage, but increasing the number of iterations should lead to a lower convergence uncertainty.
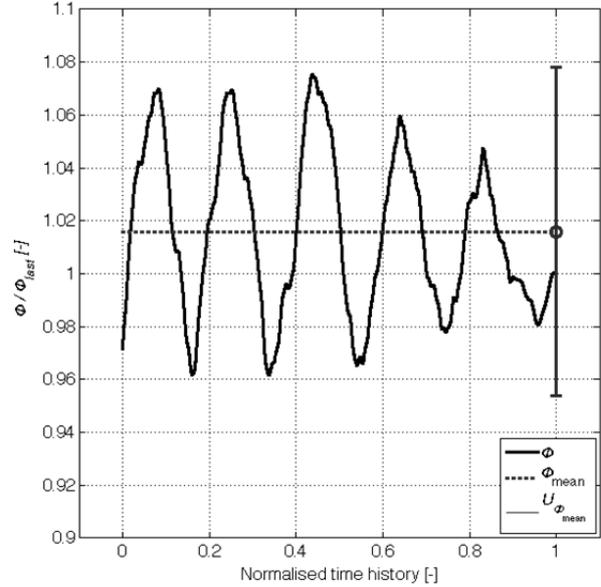

Figure 14: Convergence of the trim

3.4 VERIFICATION CONCLUSIONS

The uncertainties for the resistance (ϕ_1), sink (ϕ_2) and trim (ϕ_3), due to the grid and time resolutions, and to the convergence, are summarised in Table 3. The numerical uncertainty is computed as for Eq. (3), assuming that the round-off uncertainty is negligible because a double-precision solver was used on a 64-bit machine, and that the uncertainty due to other input parameters is also negligible.

Table 3: Summary of uncertainties

	ϕ_1	ϕ_2	ϕ_3
U_g	0.111	0.001	0.039
U_t	0.002	0.006	0.048
U_c	0.021	0.025	0.062
U_{num}	**0.132**	**0.031**	**0.124**

These results show that the numerical-experimental agreement should not be used as an indication of the simulation accuracy. In fact, despite the good agreement with the experimental results, the resistance, sink and trim are computed with uncertainties larger than 13%, 3% and 12%, respectively.

The largest uncertainty contribution is due to the 11% grid uncertainty of the resistance. In order to decrease the error, which originates this uncertainty, a finer base grid is necessary. However, without increasing the grid resolution of the base grid, the estimate of its uncertainty can be improved potentially leading to a lower uncertainty. In fact, if only finer grids than the base grid were tested, then the differences between the simulations could have been smaller. Potentially, an asymptotic trend could have been found leading to a grid uncertainty slightly higher than the difference between the results achieved with $h_g = 1$ and $h_g = 0.65$, i.e. as small as 2%.

The results showed in Section 2 show that RANS analysis can provide very useful information but its uncertainty should always be considered. The more complicated the modelled physics, the higher the uncertainty. As a rule of thumb, in free to sink and trim condition and flat water, a numerical uncertainty below 5% can be achieved. Conversely, when a yacht is modelled with six degrees of freedom, a very large uncertainty should be expected. Therefore, when a simulation is planned, it is very important to choose between more complicated simulations allowing lower modelling error but higher numerical uncertainties, and simpler simulations allowing lower numerical uncertainty and larger modelling error.

Finally, it is worth recalling that when different geometries are compared for the design purpose, the analysis of the uncertainty allows computing the level of confidence in the ranking. Interested readers can find more details in ref. [29].

3.5 VALIDATION

Table 3 shows that the numerical uncertainty is 13% of C_T, therefore $U_{C_{T\,num}} = 1.30 \cdot 10^{-3}$.

The experimental uncertainty is a combination of the uncertainty of the model-scale measurement and of the ITTC'57 model-ship correlation line and, thus, it is unknown. However, if the experimental uncertainty is assumed to be much smaller than the numerical uncertainty, then from Eq. (4) the validation uncertainty is almost equal to the numerical uncertainty, therefore $U_{C_{T\,val}} \approx 1.30 \cdot 10^{-3}$.

The numerical-experimental error, which from Table 1 is $|\delta_\phi| = 1.31 \cdot 10^{-4}$, is one order of magnitude smaller than the validation uncertainty. Therefore C_T *is validated at the level of* $U_{C_{T\,val}}$.

It should be noted that if the experimental uncertainty was under-estimated, the results would still be validated but to a higher level of uncertainty.

This example shows that stating that the results are validated is not enough, but it is important to state at which level they are validated. In fact, the larger the numerical uncertainty, the more likely the results are validated, but to the level of a higher uncertainty.

Being the results validated, it is not possible to draw any conclusion on the modelling error.

A numerical-experimental comparison performed without a rigorous V&V procedure should be considered with great caution. It is quite common that a bias due to a modelling error leads to the underestimation of the fluid dynamic forces. On the other hand, coarse grid used to model the boundary layer and low-order discretization schemes can lead to force overestimation. When these occur simultaneously, very good numerical-experimental comparison might occur hiding major errors in the simulation.

Importantly, if the experimental data is not available, the validation cannot be performed and the modelling error cannot be estimated.

4. CHOOSING A METHOD: EXPERIMENTS, POTENTIAL FLOW OR RANS

In this section, examples of applications are given with the aim of showing that the usage of experimental methods, potential flow codes and RANS codes can provide substantial benefits if used according to their features and limitations.

4.1 HULL RESISTANCE

In the early stage of the design process, potential flow codes can provide valuable information about the wave resistance. In particular, the effect of hull form factors on the wave resistance can be investigated. The main advantage of potential flow codes is the low run time required. Moreover, they can be coupled with optimisation codes in order to investigate multi-objective functions [31]. However, in most of the cases the optimum design cannot be found using these codes due to their inability to model viscous effects, and thus friction resistance and separated flow. For instance, the design with the lowest wave resistance might have a higher resistance due to separation.

In an advanced design stage, RANS codes should be used. As shown in the previous sections, the simulation might present large numerical and modelling error. Therefore, V&V are required. In order to estimate the modelling error, the experimental data is necessary. A representative design could be experimentally tested in all the conditions that have to be numerically modelled. For instance, a motor yacht can be tested at several speeds in upright condition without leeway, while a sailing yacht can be tested in several heeling and yaw conditions as well for several boat speeds. The experimental uncertainly should be estimated. Validation can then be performed on the experimentally tested design; assuming that the modelling error would not change significantly when different design candidates are modelled. When two design candidates are compared, conclusions should be drawn only if the results are validated and if the numerical uncertainty is lower than the differences between the results for the two candidates.

One of the advantages of comparing several design candidates using RANS codes instead of with only experimental tests is that the numerical results can be

more easily integrated into the design spiral. In fact, when the V&V have been performed, the resistance curve of an additional design candidate can be performed in few hours. Conversely, in order to test a new candidate in a towing tank several weeks are necessary to make the model, perform the test and receive the report. In this approach, the experimental test is performed with the aim of validating the numerical results. The numerical simulation should thus model the experimental test, at the *Fr* and *Re* used in the towing tank. The towing tank uncertainty must be known and should be taken into account in the validation uncertainty. If the numerical simulation models the full-scale condition, then the validation cannot be properly performed because the uncertainty of the methods to correct the experimental friction resistance is unknown.

4.2 APPENDAGES

Appendages can be investigated with several methods. Ventilation and cavitation on appendages can be adequately investigated with experimental tests. In particular, cavitation cannot be modelled with potential flow codes and it can be modelled with difficulty using RANS codes. During the unpublished concluding general discussion at the *Developments in Marine CFD* conference [31], it was agreed that about 50 million cells per blade are necessary to accurately model the cavitation on propellers.

The design of keels and rudders can be effectively investigated with numerical methods. Numerical methods must take into account the laminar-to-turbulent transition in order to correctly predict the resistance.

The geometry and the position of fin stabilizers are investigated with difficulty using potential flow codes and experimental methods. In fact, fin stabilizer is an airfoil with low aspect ratio and thus the viscous effects at the tip are significant. Della Rosa *et al.* [32] showed that potential flow codes increasingly underpredict the drag when the angle of attack increases. However, potential flow codes might be used for a preliminary investigation of the two-dimensional section of the fin. Experimental tests might be difficult because the drag of the fin stabilizer is significantly lower than the drag of the entire hull. The investigation of the position of the fin involves the study of the streamline along the hull, which could be done both with RANS codes and experimentally.

As an example, the authors designed a two-dimensional section of a fin stabilizer using the potential flow code XFOIL coupled with a genetic algorithm based code [32]. The design objectives were the maximum lift/drag ratio at three degrees angle of attack, and the maximum lift. The optimum

section was then used to design the three-dimensional fin, which was modelled with STAR-CCM+ (CD-adapco). The analysis of the fin in isolation allowed the design of the end-plate, sweep angles and taper ratio. The zero-speed condition was also modelled. When the yacht is at anchor, the fin can rotate of about 60 degree in 10 seconds leading to a significant roll moment, which can be used to counteract the roll moment due to waves. Additional analysis was performed in order to investigate the best fin-hull configuration. The hull was the 105-foot power yacht presented in Section 2. Two possible configurations were considered: one fin per side and two fins per side (Figure. 15).
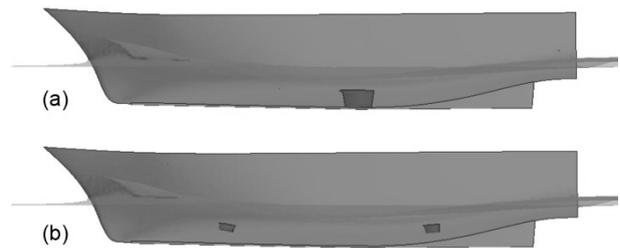

Figure 15: Fin's position and geometrical alignment. (a) one fin per side; (b) two fins per side.

The fins used in the two configurations were geometrically similar but were scaled in order to keep the same wetted surface and not to increase the maximum draft and beam of the hull. A multiphase RANS analysis performed with a similar setup than the one described in Section 2 allowed the streamlines along the hull to be computed at several yacht speeds considering the free-surface effect, and thus to align the fins in order to avoid wake interference. The difference in the resistance computed for the two configurations was of the order of 1% and lower than the simulation uncertainty.

4.3 PROPELLERS

In the simulations presented in Section 3 the propulsor has not been modelled. However, it has a significant impact on the velocity and pressure distributions on the hull and on every downstream appendage. For instance, the wake of a propeller on a rudder can alter the efficiency of the rudder thus the circulation due to it. Vice versa, the boundary layer on the hull leads to a non-uniform onset flow experienced by the propulsor. This coupled interaction can be modelled with RANS, but from a design point of view, this is too computationally expensive. For conventional propellers, for instance, the rotation of the blade requires the use of sliding meshes, and the grid resolution near the blade tip must be higher than the one in the boundary layer of the hull.

RANS and potential flow codes can be used together efficiently if the flow around the hull is modelled with a

RANS code and the flow at the propeller disk is transferred to the potential flow code which model the propeller. For instance, Villa *et al.* [33] developed a coupled method where the RANS solution at the disk is transferred to the potential flow coded as equivalent body forces. A simpler approach is modelling within the RANS code the axial momentum of the propulsor and, potentially, take also into account each individual blade element.

Cavitation can be explored very efficiently with model-scale tests in cavitation tunnels. For instance, the Emerson Cavitation Tunnel at the Newcastle University has a test section 3.10 x 1.22 x 0.81 m and can test different kind of propulsors up to 0.4 m in diameter. The maximum velocity of 10 m/s and pressures from 7.6 to 106 kN/m^2 allow reaching cavitation numbers from 0.5 to 2.

As an example, the authors performed a RANS investigation of a 163-foot motor yacht with two propeller shafts using the code Fluent (Ansys Inc.) [34]. In order to save computational time without compromising the spatial resolution, a multi-phase simulation of the yacht without the propeller shafts was performed in a free to sink and trim condition. Then a subdomain near the propeller shafts was identified. The solution of the multi-phase simulation was used to set the boundary conditions of the mono-phase simulation modelling the subdomain with the propeller shafts (Figure. 16), taking into account the trimmed and sunk position of the hull, and the disturbed free surface. A steady RANS simulation using the $k - \omega\ SST$ turbulence model was performed. In particular, only the half body was modelled using the symmetry plane of the yacht and a tetrahedral grid of about 2.3 million cells was made with Gambit and Tgrid (Ansys Inc.). The grid was refined in order to achieve y+ of the order of 60 both along the hull and on the appendages. The effect of the accentuated longitudinal curvature of the hull in correspondence of the propeller disks on the velocity and pressure fields was investigated.
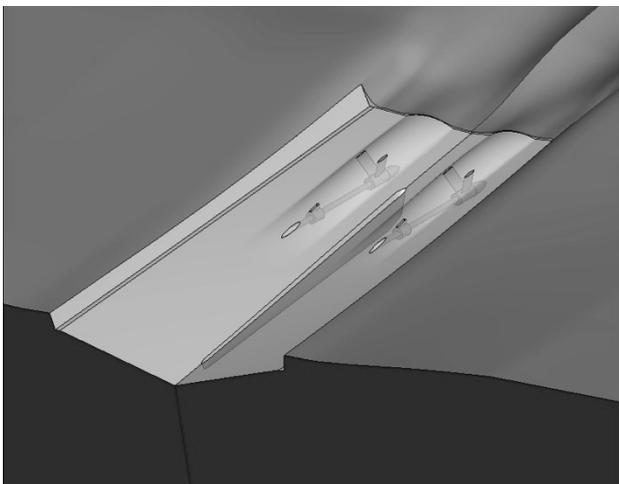

Figure 16: Subdomain near the propeller shafts [34].

Figure 17 shows the dynamic pressure (divided by the inlet dynamic pressure) on the longitudinal plane of a propeller shaft. The velocity and pressure fields at the propeller disk were then used by the Department of Naval Engineering, Universita' degli Studi di Genova, as input for the potential flow code modelling of the propeller [35].
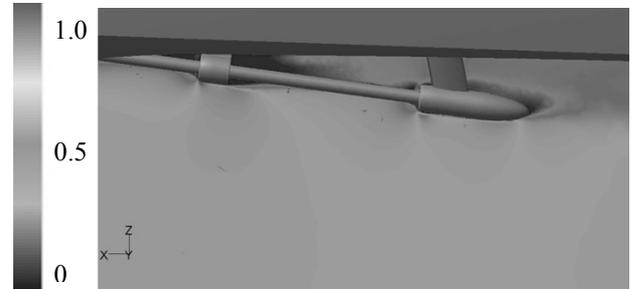

Figure 17: non-dimensional dynamic pressure on the longitudinal plane [34].

5.   CONCLUSIONS

The paper discusses the features and the limitations of numerical methods in yacht design.

RANS codes are particularly computational demanding and therefore their usage increased with the grown of computational resources. In the recent years, the capabilities of RANS codes have been thoroughly investigated while the associated uncertainty of the numerical results have been often underestimated. The quality and the reliability of a simulation are often and dangerously assessed by the numerical-experimental difference, instead of on the estimate of the numerical and modelling errors, i.e. on the validation uncertainty.

RANS codes can model a very wide range of complex physics, but the spatial and time resolutions required to achieve small uncertainty can be extremely high. Also, the uncertainty due to the convergence can significantly increase the final uncertainty of the computed solution. In general, the higher the complexity of the simulation, the higher the uncertainty of the result.

The paper showed that simulations allowing numerical-experimental agreement of the order of 1% may well be affected by uncertainty of the order of 10%. The overall quality and reliability of the simulation can only be assessed by the validation uncertainty, which shows the level at which the simulation is validated.

Similar considerations can be applied to potential flow codes. However there is more awareness of the potential flow code limitations than the RANS code limitations.

The main advantage of RANS codes is their capability of modelling viscous phenomena, which potential flow codes cannot do. Moreover, RANS codes provide the

velocity and pressure fields in the entire computational volume while typical commercial potential flow codes provide the velocity and pressure fields on three-dimensional surfaces. The main draw back is the longer run time and the higher expertise required to correctly setup the simulation.

Experimental tests are fundamental to perform the validation of the numerical codes. Moreover, in some applications the experimental uncertainty can be very low and the same uncertainty can be achieved with difficulties with numerical methods. For instance, cavitation can be tested in a cavitation tunnel and very accurate measurements can be performed, while RANS codes require a very high spatial and time resolutions in order to achieve the same uncertainty.

Each of the three methods has their own unique features and they must be used with a thorough understanding of their limitations, so as to provide a reliable suite of design tools.

6. ACKNOWLEDGMENTS

7. REFERENCES

1. FROUDE, W., Report to the Lords Commissioners of the Admiralty on experiments for the determination of the friction resistance of water on a surface, under various conditions, performed at Chelson Cross, under the authority of Their Lordships, *44th Report of the British Association for the Advancements of Science, pp 249-255,* 1874.
2. PRANDTL, L., Bericht über Untersuchungen zur ausgebildeten Turbulenz, *Z. Angew, Math, Meth., vol 5, pp 136-139,* 1925.
3. VON KÁRMÁN, T., Über laminare und turbulente Reibung, *Z. Angew. Math. Mech., vol 1, pp 233-252,* 1925 *(English translation in NACA Technical Memo.* 1092*)*.
4. BLASIUS, H., Grenzschichten in Flüssikeiten mit kleiner Reibung, *Z. Angew. Math. Phys., vol 56, pp 1-37,* 1908 *(English translation in NACA Technical Memo.* 1256*)*.
5. HUGHES, G., Frictional resistance of smooth plane surfaces in turbulent flow, *Trans. Inst. Naval Archit., vol 94, pp. 287-322,* 1952.
6. HUGHES, G., Friction and form resistance in turbulent flow and a proposed formulation for use in model and ship correlation, *Trans. Inst. Naval Archit., vol 96,* 1954.
7. International Towing Tank Conference, 8th ITTC, Madrid*, Canal de Experiencias Hidrodinamicas, El Pardo, Madrid, Spain,* 1957.
8. NAVIER, C.L.M.H., Mémoire sur les lois du mouvement des fluides, *Mem. Acad. R. Sci. Paris*, *vol 6, pp 389-416,* 1823.
9. STOKES, G.G., On the theories of the internal friction of fluids in motion, and of the equilibrium and motion of elastic solids, *Trans. Camb. Phil. Soc., vol 8, pp 287–305,* 1845.
10. SPALART, P.R., Direct simulation of a turbulent boundary layer up to $Re\theta = 1400$, *J. Fluid Mech., vol 187, pp 61-98,* 1988.
11. HEDGES, K.L., Computer Modeling of Downwind Sails, *New Zealand, University of Auckland, ME Thesis, 85 pp,* 1993.
12. MIYATA, H., LEE, Y.W., Application of CFD Simulation to the Design of Sails, *J. Mar. Sci. Technol, vol 4, pp 163-172,* 1999.
13. VIOLA, I.M., Downwind Sail Aerodynamics: a CFD Investigation with High Grid Resolution, *Ocean Eng, vol 36(12-13), pp 974-984,* 2009.
14. VIOLA, I.M., PONZINI, R., A CFD Investigation with High-Resolution Grids of Downwind Sail Aerodynamics, *RINA Intl. Conf. on Developments in Marine CFD, London, UK, RINA, pp 99-110, 22-23 Mar,* 2011.
15. KODAMA, Y., TAKESHI, H., HINATSU, M., HINO, T., UTO, S., HIRATA, N., MURASHIGE, S. (editors), *Proc. of CFD Workshop Tokyo 1994: An Intl. Workshop for Improvement of Hull Form Designs, Ship Res. Inst., Tokyo, Japan, 2 vols, 22-24 March,* 1994.
16. LARSSON, L., REGNSTROM, B., BROBERG, L., LI D-Q., JANSON, C-E, Failures, Fantasies and Feats in the Theoretical/Numerical Prediction of Ship Performances, *22nd Symp. on Naval Hydrodynamics, NAP, Washington, C, USA, pp 11-32, Aug,* 1998.
17. ORIHARA, H., MIYATA, H., CFD Simulation of a Semi-planing Boat in Unsteady Motion*, 4th International Conf. on Fast Sea Transportation (FAST '97), Sydney, Australia. Baird Publications, vol 1, pp 35-42, Jul,* 1997.
18. MIYATA, H., AKIMOTO, H., HIROSHIMA, F., CFD erformance Prediction Simulation for Hull-form Design of Sailing Boats, *J. Mar. Sci. Technol., vol 2, pp 257-267,* 1997.
19. AZCUETA, R.R., Computational of Turbulent Free-surface Flows Around Ships and Floating Bodies, *Technishen Universitat Hamburg-Harburg, Doktor-Ingenieur genehmigte Disseratation, PhD thesis, 105 pp,* 2001.
20. HINO, T. (editor), The Proc. of the CFD Workshop Tokyo 2005*, National Maritime Res. Inst., Tokyo, Japan, 9–11 March*, 2005.
21. LARSSON, L., STERN, F., BERTRAM, V., Benchmarking of Computational Fluid Dynamics for Ship Flows: the Gothenburg 2000

Workshop, *J. Ship Res, vol 47(1), pp 63–81, March,* 2003. www.gothenburg2010.org

22. CD-adapco, User Guide STAR-CCM+ Version 4.06.011, CD-adapco, 2009.

23. ROACHE, P., Perspective: a Method for Uniform Reporting of Grid Refinement Studies, *ASME J. Fluids Eng, vol 116, pp 405-413,* Sept 1994.

24. RAHAIM, C.P., OBERKAMPF, W.L., COSNER, R.R., DOMINIK, D.F. AIAA Committee on Standards for CFD-Status and Plans, *41st Aerospace Sciences Mtg, Reno, Nevada, USA, Paper AIAA-2003-844, 6–9 Jan,* 2003.

25. AIAA, Guide for the Verification and Validation of Computational Fluid Dynamics Simulations, *USA; Guide AIAA-G-077-1998, 19 pp,* 1998.

26. ASME. Standard for Verification and Validation in Computational Fluid Dynamics and Heat Transfer, *USA, ASME, VV20-2009, 88 pp,* 2009.

27. FREITAS, C.J., GHIA, U., CELIK, I., ROACHE, P., RAAD, P., ASME's Quest to quantify numerical uncertainty, *41st Aerospace Sciences Mtg, Reno, Nevada, USA, Paper AIAA-2003-627, 6–9 Jan,* 2003.

28. ITTC, The Resistance Committee, Uncertainty Analysis in CFD, Verification and Validation Methodology and Procedures, *23rd Intl. Towing Tank Conf., Venice, Italy, ITTC-Quality Manual, CFD General, 7.5-03-01-01, 8-14 Sept,* 2002.

29. VIOLA, I.M., BOT, P., RIOTTE, M., On the Uncertainty of CFD in Sail Aerodynamics, *International Journal for Numerical Methods in Fluids, vol. 72(11), pp. 1146-1164, 20 Aug 2013.*

30. VIOLA, I.M., FLAY, R.G.J., PONZINI, R., CFD Analysis of the Hydrodynamic Performance of Two Candidate America's Cup AC33 Hulls, *International Journal of Small Craft Technology, Trans. RINA, vol 154(B1), pp 1-12,* 2012.

31. Royal Institution of Naval Architects, Proceedings of Developments in Marine CFD, *London, UK, 23-24 March,* 2011.

32. DELLA ROSA, S., MACERI, M., VIOLA, I.M., BARTESAGHI, S., Design and Optimization of a Fin Stabilizer Using CFD Codes and Optimization Algorithms, *Nav 2009. 16th Intl. Conf. of Ship & Shipping Research, ATENA, Messina, Italy. Italy, 26-27 Nov,* 2009.

33. VILLA, D., GAGGERO, S., BRIZZOLARA, S., Simulation of Ship in Self-Propulsion with Different CFD Methods: From Actuator Disk to Potential Flow coupled solvers to fully unsteady RANS model, *Intl. Conf. on Developments in Marine CFD, RINA, London, UK, pp 1-12, 22-23 Mar,* 2011.

34. DELLA ROSA, S., VIOLA, I.M., BARTESAGHI, S., CFD analysis of the hydrodynamic performance of Aifos 163', *Report for Hydro Tec., Della Rosa Naval Architect, Milan, Italy, April,* 2009.

35. BRIZZOLARA S., Propeller performance analysis for Hydro Tec, *Report for Hydro Tec., Dipartimento di Ingegneria Navale, Universita' degli Studi di Genova, Italy,* 2009.